Report Title: Materials System for Intermediate Temperature Solid Oxide Fuel Cell

Type of Report: Annual Technical Progress report

Reporting Period Start Date: 9/26/02

Reporting Period End Date: 9/25/03

Principal Author(s): Professors Uday B. Pal and Srikanth Gopalan

Dated: February 15, 2004

DOE Award Number: DE-FG26-02NG41539

Department of Manufacturing
15 St. Mary's Street
Boston University, MA 02446

Abstract

AC complex impedance spectroscopy studies were conducted on symmetrical cells of the type [gas, electrode/LSGM electrolyte/electrode, gas]. The electrode materials were slurry-coated on both sides of the LSGM electrolyte support. The electrodes selected for this investigation are candidate materials for SOFC electrodes. Cathode materials include $La_{1-x}Sr_xMnO_3$ (LSM), LSCF ($La_{1-x}Sr_xCo_yFe_{1-y}O_3$), a two-phase particulate composite consisting of LSM + doped-lanthanum gallate (LSGM), and LSCF +LSGM. Pt metal electrodes were also used for the purpose of comparison. Anode material investigated was the Ni + GDC composite. The study revealed important details pertaining to the charge-transfer reactions that occur in such electrodes. The information obtained can be used to design electrodes for intermediate temperature SOFCs based on LSGM electrolyte.

Table of Contents

List of Graphical Materials

Introduction

Solid oxide fuel cells (SOFCs) offer the possibility of very high efficiency power generation. They are noiseless, emit far lower quantities of greenhouse gases such as CO_2 compared to conventional power generation systems, have virtually zero NO_x and SO_x emissions. Despite their many advantages, SOFC power systems are not yet cost-effective to merit large-scale deployment in the power generation industry. Of the approaches currently being investigated to decrease the cost of SOFCs, improving power density while decreasing operating temperature is perhaps the most promising option. Improvements in power density will result in decreased system size**,** which in turn will have the effect of decreasing the size of the balance of plant (BOP). Decreasing operating temperature will lead to the deployment of cheaper manifolding and interconnection materials. However, decreasing operating temperature has the effect of increasing all types of polarization losses in the cell. Thus the simultaneous goals of improving power density while lowering the operating temperature are at odds with each other. Therefore, the focus of recent research is aimed at development of more active electrodes and more conductive electrolyte materials that can efficiently operate at lower temperatures (600-800 ^oC).

A very large fraction of the total polarization losses is known to occur at the electrode-electrolyte interfaces manifesting itself as the kinetic barrier to charge-transfer reactions. Great advances have been made in reducing electrode polarization related to the charge-transfer reaction through the use of two-phase porous composite electrodes [1-4] and mixed conducting electrodes [5]. Much of this work has been aimed at developing electrodes for SOFCs based on the conventional yttria stabilized zirconia (YSZ) electrolyte. The focus of this paper is an investigation of electrode materials for SOFCs based on the perovskite electrolyte $La_{1-x}Sr_xGa_{1-y}Mg_yO_3$ (or LSGM). LSGM has received a lot of interest in recent years after it was first reported by Goodenough et al. [6] to have significantly higher oxygen-ion conductivity than conventional YSZ.

It is generally accepted that high power densities in SOFCs can be achieved only through employment of electrode-supported cells rather than electrolyte-supported cells. There are essentially two-options in the design of electrode-supported cells, namely, cathode- and anode-supported SOFCs. Schematics of the two designs are shown in Figure 1. In both designs, it is suggested that coarser-grained electrodes with coarser connected porosity be employed away from the electrolyte-electrode interfaces while finer-grained electrodes with finer connected porosity used closer to the electrolyte-electrode interfaces. The coarser porosity away from the electrolyte-electrode interface facilitates gas transport and the finer porosity closer to the interfaces aids in the charge-transfer reactions. This paper reports measurements of polarization resistances for various materials for potential application as the finer microstructured layer near the electrolyte-electrode interface as shown in Figure 1. The list of electrode materials investigated in this study is given in Table 1.

AC complex impedance spectroscopy has been used to measure the effective charge-transfer polarization at the electrode-electrolyte interfaces using symmetrical cell arrangements. The experimental technique is described in the following section.

Executive Summary

The objective of the proposed research is to investigate a materials system for intermediate temperature solid oxide fuel cell that is capable of operating between 500-700^{0}C with a power density greater than 0.6W/cm^2 at 0.7V. The electrolyte, anode, and cathode materials in the SOFC system being investigated are based on lanthanum gallate ($La_{1-x}Sr_xGa_{1-y}Mg_yO_{3-\delta}$ or LSGM), nickel-ceria ($Ce_{0.9}Y_{0.1}O_{2-x}$) cermet, and LSGM-lanthanum cobaltite ($La_{0.8}Sr_{0.2}CoO_3$, or LSC) composite, respectively. These material choices are based on their property information available in the literature, which indicate that they meet the operational requirements of the intermediate-temperature SOFC.

Interfacial polarizations of the candidate electrodes for the $La_{0.9}Sr_{0.1}Ga_{0.8}Mg_{0.2}O_3$ (LSGM) electrolyte have been investigated by Impedance spectroscopy technique.

Among the cathode materials (LSM ($La_{0.85}Sr_{0.15}MnO_3$), LSM-LSGM and $La_{1-x}Sr_xCo_yFe_{1-y}O_3$ (LSCF)), the pure LSM electrode had the worst polarization performance. The addition of LSGM electrolyte material to the LSM electrode increases the mixed-conducting boundary with the gas phase and lowers the overall polarization. Although LSM-LSGM composite electrodes are better than just pure LSM, the performance of the best LSM-LSGM (40:60) electrode was similar to that of platinum. Single-phase mixed-conducting LSCF electrode had three orders lower polarization resistance than the LSM-LSGM composite electrodes. Addition of LSGM to LSCF did not significantly alter (lower) the polarization resistance of the LSCF electrodes. However, a composite LSCF-LSGM (40:60 by volume) electrode is preferred over plain LSCF electrode in order to match the coefficient of thermal expansion with the LSGM electrolyte and reduce the residual stresses. It is also observed that the interfacial polarization resistance of the LSCF electrode decreased asymptotically as the electrode thickness is increased. However, it is anticipated that above a certain electrode thickness mass-transfer polarization will start to dominate and increase the overall polarization. Therefore if the cathode is not used as a supporting electrode then it requires a certain minimum thickness (30-40 micrometers) with finer electrode porosity to lower the interfacial polarization.

The anode material investigated was Ni-Gadolinium doped Ceria (Ni-GDC). It was observed that the LSGM electrolyte reacts with the Ni during processing and also at the operating temperature and increases the polarization resistance. A dense buffer layer of GDC between the LSGM electrolyte and the Ni-GDC composite anode prevents this interaction and a much lower electrode polarization is observed. However, it is important to keep the temperature below 1200 degree C during electrode sintering or firing otherwise there appears to be an interaction between the LSGM and the GDC buffer layer. Different methods of anode manufacture are being investigated. Effects of Ni-GDC anode composition, structure and thickness on interfacial polarization will be investigated once the optimum anode manufacturing process is standardized.

After determining the optimum electrode composition, structure and thickness of the cathode and the anode with respect to the LSGM electrolyte, complete anode-supported planer cells will be fabricated and evaluated in terms of its I-V characteristics and component stability.

Experimental

Powder synthesis: Powders of the composition $La_{0.9}Sr_{0.1}Ga_{0.8}Mg_{0.2}O_3$ (LSGM) were synthesized by mixing high purity precursors of lanthanum carbonate, strontium carbonate, gallium oxide and magnesium oxide in appropriate stoichiometric ratios and calcining at a temperature of 1200°C for 4 hours in air. Electrode materials such as $La_{0.9}Sr_{0.1}MnO_3$ (LSM), $La_{0.6}Sr_{0.4}Co_{0.8}Fe_{0.2}O_3$ (LSCF), and $Ce_{0.85}Gd_{0.15}O_2$ (GDC) were also made using the same mixing and calcination techniques. The calcined powders were lightly crushed using alumina mortar and pestle and the calcination step was repeated for completing the solid-state reaction. X-ray powder diffraction analysis confirmed the composition, phase and purity of the material. All the synthesized powders (LSGM, LSM, LSCF, GDC) and NiO powder purchased from Baker were then separately ball-milled in methanol. Laser Scattering Particle Size Distribution Analyzer (Horiba LA-910) was periodically used at different intervals of the ball milling process to determine the particle size and distribution. The ball milling process was stopped when the desired particle size and distribution were obtained. The final particle size and distribution of all the powders are shown in Fig. 2.

Symmetrical cell fabrication: Calcined and milled LSGM powders at room temperature were die-pressed with 10000 psi pressure into pellets and sintered in air at 1450°C for 4 hours. The sintered LSGM pellets were 1.4 mm thick and 2 cm in diameter. The LSGM pellets were then all finely ground to a uniform 1 mm thickness using diamond grinding discs. LSM-LSGM, LSCF-LSGM, NiO-GDC composite electrodes were prepared by thoroughly mixing controlled amounts of powders. The electrode powders (LSM, LSM-LSGM, LSCF, LSCF-LSGM, NiO-GDC) were each dispersed in α-terpeniol solvent to form a paste. The ground LSGM electrolyte pellets were masked with Scotch™ tape to form an outer ring on both sides and the electrode pastes were painted smoothly on the open circular surfaces. The painted electrolyte pellets were air dried, masks removed and fired in air at elevated temperature for 2 hours. The firing temperature was 1100°C for all the cathodic samples and 1300°C for the anodic (i.e. NiO-GDC electrode sample). When platinum electrodes were used, commercial platinum paste (6926 Engelhard) was painted over a similarly masked LSGM electrolyte pellet, air dried, masks removed and fired at 950°C for 2 hrs. All electrodes had the same effective area of around 1.33cm^2. For the cathode materials, two pieces of platinum mesh were co-sintered on both electrode surfaces at the same time to act as current collectors. Lead wires of Pt were used to connect the platinum mesh current collectors to the measuring instrument. For the anode materials, Nickel mesh was pressed over the electrode surfaces in a reducing atmosphere, and lead wires of Nickel were used

AC impedance characterization: The experimental setup that was used is shown in Figure 3. In this setup the symmetrical cell was exposed to the same oxidizing (cathodic), or reducing (anodic) atmosphere on both sides and a two-probe configuration was used to measure the impedance spectra. During measurement a constant flow rate of air was maintained for experiments involving the cathode materials, and a constant flow rate of forming gas, i.e. 95% argon-5% hydrogen bubbled through water at 25°C was maintained for experiments involving the anode materials The measurements were made by applying a small-amplitude AC voltage (10mV) to the cell and monitoring the response current as a function of the AC frequency (from 1 mHz to 65 KHz). A plot of the

imaginary part of the measured impedance versus the real part reveals details of the individual ohmic and polarization contributions to the total resistance of the cell. Impedance measurements were made in the temperature range of 600 to 800^{o}C in 50^{o}C increments for all the samples using a Perkin-Elmer potentiostat/galvanostat (263A) and solartron analytical frequency response analyzer (model 1250).

These impedance measurements were performed both as a function of composition for LSM-LSGM electrodes and as a function of electrode thickness for the LSCF electrodes. After electrochemical testing, the samples were epoxy mounted and polished in cross section; both SEM and optical microscopy were used to measure the grain size, porosity and thickness of the electrodes and confirm the consistency of the microstructure.

Results and Discussions

Microstructure: Typical SEM pictures of the fracture surface of the electrodes LSM, LSM-LSGM, LSCF, LSCF-LSGM and their interfaces with the electrolyte are shown in Fig.4. The cross sections in Fig. 4 show that these electrodes have similar microstructures in terms of their interfacial adherence with the LSGM electrolyte, porosity and grain size. The backscattered SEM pictures of epoxy mounted and polished LSM, LSM-LSGM, and LSCF electrodes are shown in Fig. 5. The grain size is on the order of 1-2 μm and the porosity of LSM, LSM-LSGM, LSCF electrode are 55.5%, 54.3%, and 53.3% respectively measured in terms of percentage area of the pores in the micrographs using Adobe Photoshop software. Based on the porosity measurement, gas diffusion is not expected to control the polarization process particularly for small applied potentials that were used for the AC impedance measurements.

Impedance spectroscopy: A typical impedance plot measured using the symmetrical cell arrangement with LSCF electrodes is shown in Figure 6. As discussed elsewhere by previous workers [7, 8, 9, 10, 11, 12, 13], the high-frequency intercept of the impedance spectrum gives the ohmic resistance of the cell (R_s), which includes the resistive contributions of the electrolyte, the two electrodes, the current collectors and the lead wires. The low-frequency intercepts gives the total resistance ($R_s + R_p$), which includes the ohmic resistance of the cell, concentration polarization (or mass transfer polarization) resistance and the effective charge-transfer polarization resistance (R^{eff}_{ct}) and any other type of polarization resistance arising from adsorption effects. The total polarization resistance of the electrode (R_p) is then extracted from the impedance plot. For all samples measured in this investigation, a single depressed arc was observed. Given that the electrodes are thin, the amplitude of the applied AC voltage is small (10mV), and the air flow over the electrode was continuous, it is most likely that the effective charge transfer resistance, R^{eff}_{ct}, dominates the polarization resistance for the electrodes, i.e. the concentration polarization is negligibly small and R_p is essentially equal to R^{eff}_{ct}.

Effect of cathodic LSM-LSGM electrode composition on polarization resistance: The typical AC impedance spectra of LSM-LSGM/LSGM/LSM-LSGM symmetrical cells (about 30 μm thickness) tested at 800^{o}C in air is shown in Fig. 7. It is evident from this figure that when the LSGM content in the electrode is below 70 w%, the high frequency intercepts remained the same, indicating that the effective composite electrode/electrolyte interfacial contact area is roughly the same. However, an increase in the LSGM content resulted in a decrease of the polarization resistance, which was due to

the increased mixed conducting TPB area within the electrode. When the LSGM content was more than 70 w%, which is the percolation threshold, the ohmic resistances of the electrodes were no longer negligible and therefore the high-frequency intercept of the impedance spectra was much larger (Fig. 7). The temperature dependence of the polarization resistance for different LSM-LSGM compositions is shown in Fig. 8. The activation energies as a function of LSM-LSGM composition obtained from Fig. 8 are shown in Table 2. The activation energies increased with the LSGM content, from 126KJ/mol for pure LSM to 182KJ/mol for the 40/60 LSM-LSGM electrode. This suggests that the composite electrode was becoming more ionic conducting in character as the LSGM content was increased and it was also resulting in lowering the polarization resistance of the electrode within the percolation threshold.

Effect of electrode on cathodic polarization resistance: The Arrhenius plot of the measured polarization resistance for the various cathode materials, listed in Table 1, are shown in Figure 9. It is to be noted that the ohmic resistance, R_s, obtained from the high-frequency intercept of the impedance spectra, was approximately the same for all these electrodes indicating that the effective electrode/electrolyte interfacial contact area for these electrodes were similar. As can be seen in Figure 9, the standard 30 μm thick LSM cathode has a polarization resistance which is worse than the 5 μm thick Pt electrode. The 30 μm LSM-LSGM (40:60) composite electrode has a polarization resistance that is very similar to the Pt electrode. In contrast the 30 μm thick LSCF electrode has a polarization resistance which is six orders of magnitude lower than the Pt, LSM and LSM-LSGM electrodes. For the 30 μm LSCF-LSGM (50:50) composite electrode, the polarization resistance was slightly smaller than that of pure 30 μm LSCF electrode. This can be rationalized on the premise that single-phase LSCF already has a high ionic conductivity. However, adding LSGM to the LSCF electrode can buffer the thermal expansion coefficient of the electrode so as to close the TEC gap between LSGM and LSCF materials. The activation energies of these electrodes are listed in table 3. These values do suggest that both the catalytic behavior and the ionic conductor constituent of the electrodes influence the activation energies.

Effect of LSCF electrode thickness on effective charge-transfer resistance: AC impedance spectra of LSCF/LSGM/LSCF symmetrical cells at 600^{o}C as a function of electrode thickness are shown in Figure 10. All the impedance arcs as stated earlier appeared to be semicircle in nature, and the polarization resistance changed with the thickness of the electrodes. It is evident from Figs. 10 and 11 that increasing the electrode thickness has the effect of decreasing the effective charge-transfer resistance. A similar thickness effect has been observed previously by Kenjo et al. [2, 14] and Tanner et al. [15, 16]. Tanner et al. [15] developed a comprehensive model to explain the thickness effect of the effective charge-transfer resistance of LSM-YSZ composite electrodes on YSZ electrolytes. When the electrocatalyst cathode is a pure electronic conductor like LSM, the sites for charge-transfer reactions have been conclusively shown by Horita et al. [17] using oxygen-18 isotope and secondary ion mass spectrometry (SIMS) to be the three-phase boundaries (TPBs) formed between the electrode (LSM), electrolyte (YSZ) and the gas-phase. Thus, in the case of a porous composite electrode comprising an electrocatalyst phase (LSM), and an ionic conducting phase (YSZ) it is reasonable to expect that increasing the electrode thickness should lead to an increase in the TPB line length and therefore a decrease in effective charge-transfer resistance eventually approaching an

asymptotic minimum. Indeed the experimental and theoretical work of Tanner et al. [15, 16] showed just such a thickness effect.

In the case of a single-phase mixed ionic and electronic conducting (MIEC) electrode, in addition to the TPBs at the electrode-electrolyte interface, oxygen exchange can occur over the entire pore surface area of the electrode. The nature of this oxygen exchange, i.e. whether it is electrochemical (charge-transfer) or simply a chemical exchange process is the subject of much recent debate [18, 19]. The results presented here do not throw light on this debate. However, regardless of the nature of the oxygen exchange process, an increase in MIEC electrode thickness should reduce the total polarization resistance by increasing the number of sites available for exchange between the gas phase and the electrode-electrolyte system just as in the case of porous composite electrodes [15]. As can be seen from Figure 11, this is indeed the case observed in this study involving the LSCF/LSGM/LSCF symmetrical cells. Figure 11 also shows a fit to our data using the model developed by Tanner et al. [15] using porosity (53.3%), intrinsic charge transfer resistance R_{ct} (3.8 Ω. cm^2), ionic conductivity (0.025 s/cm) and grain size (1 μm). This also confirms our initial hypothesis that concentration polarization is a minor contributor to the total polarization resistance in our experiments. Upon further increasing the electrode thickness, pore diffusion of molecular oxygen through the MIEC electrode phase may become rate controlling and therefore increase the total electrode polarization resistance. Indeed, this effect has been predicted by Tanner et al. [15]. However, such an increase in R^{eff}_{ct} was not observed in the electrode thickness range investigated in this study (4.5 μm to 150 μm**)**. This once again confirms our hypothesis that the electrodes investigated in this study were not rate-controlled by gas-phase pore diffusion.

The effect of microstructure changes on effective charge-transfer resistance has not been investigated in this study. But, it can be expected that a finer micro-structured electrode is expected to lead to a lower effective charge-transfer resistance due to the availability of greater number of sites for charge-transfer reactions. As shown theoretically by Tanner et al. [15], the thickness at which the asymptotic minimum in the effective charge-transfer resistance is attained for a given electrode depends on the microstructure of the electrode; finer the electrode microstructure smaller the electrode thickness at which the asymptotic minimum is attained. This behavior will also be dependent on the mixed conducting characteristics of the electrode. These are some of the other cathodic polarization issues that are being investigated and will be the subject of future publications.

Effect of alternate transport paths on effective charge-transfer resistance: In the model developed by Tanner et al. [15] for two-phase composite electrodes (e.g. LSM-YSZ) it has been assumed that the charge-transfer process occurs at the TPBs at the electrode, electrolyte and gas interfaces. In their calculations Tanner et al. [15] replaced the TPBs by a negligibly thin continuous region where charge-transfer occurs. One of the assumptions in their model is that once oxygen ion formation occurs at the TPBs, the only path for transporting it is through the contiguous electrolyte grains extending into the electrode. While this may be true in some cases, alternate transport paths for the oxygen ions, e.g. ambipolar surface transport in the MIEC electrodes may also be possible and should be considered. Presently we are refining the model by Tanner et al. [15] to incorporate such alternate transport paths which will the subject of a future publication.

Effect of reaction between nickel anode material and LSGM electrolyte on polarization resistance: Nickel is a well-known SOFC anode material, and acts as the fuel

side electrocatalyst and current collector. Ni-GDC cermet anode is known to be an effective anode for SOFCs based on LSGM electrolyte [20]. However, upon maintaining a Ni-GDC/LSGM/Ni-GDC symmetrical cell in the same reducing atmosphere at 800^{o}C, both the ohmic resistance and polarization resistance increased gradually with time, which is shown in Figure 12 and 13. These results confirm prior results that Ni reacts with LSGM forming insulating phases (lanthanum nickelates) at elevated temperatures [21]. GDC is an excellent oxygen ionic conductor and is chemically and mechanically compatible with the LSGM electrolyte. Thus an intermediate dense layer of GDC should be used between the LSGM electrolyte and Ni-GDC anode to prevent direct contact between the Ni in the anode and the electrolyte. This is the focus of ongoing work in our lab.

Conclusions

Charge-transfer polarization of several candidate electrodes for LSGM electrolyte has been investigated by Impedance spectroscopy technique. Among these cathode materials (LSM, LSM-LSGM and LSCF), the pure LSM electrode has the worst polarization performance. The addition of LSGM electrolyte material to the LSM electrode increases the mixed-conducting boundary with the gas phase and lowers the polarization. Although LSM-LSGM composite electrodes are better than just pure LSM, the performance of the best LSM-LSGM (40:60) electrode was similar to that of platinum. Single-phase mixed-conducting LSCF electrode has much lower polarization resistance than the LSM-LSGM composite electrodes. As expected, the polarization resistance of the LSCF electrode decreased asymptotically as the electrode thickness is increased. Although adding LSGM electrolyte material to the LSCF electrode doesn't improve the cell performance very much, it can buffer the larger thermal expansion coefficient of LSCF compared to the LSGM electrolyte. As the anode material, Ni, reacts with LSGM electrolyte and lowers the overall cell performance, a dense layer of GDC between LSGM electrolyte and Ni-GDC anode is necessary.

References

1. T. Kawada, N. Sakai, H. Yokokawa, M. Dokiya, M. Mori and T. Iwata: "Characteristics Of Slurry Coated Nickel Zirconia Cermet Anodes for Solid Oxide Fuel Cell," *J. Electrochem. Soc.,* 1990, 137, pp. 3042-3046.
2. T. Kenjo and M. Nishiya: "$LaMnO_3$ air cathodes containing ZrO_2 electrolyte for high temperature solid oxide fuel cells," *Solid State Ionics,* 1992, 57, pp. *295-302.*
3. M.J.L. Østergård, C. Clausen, C. Bagger and M. Mogensen: "Manganite-zirconia composite cathodes for SOFC: Influence of structure and composition," *Electrochim. Acta,* 1995, 40, pp.1971-1981.
4. V. Dusastre and J. A. Kilner: "Optimisation of composite cathodes for intermediate temperature SOFC applications," *Solid State Ionics*, 1999, 126, pp.163-174.
5. M. T. Colomer, B. C. H. Steele and J. A. Kilner: "Structural and electrochemical properties of the $Sr_{0.8}Ce_{0.1}Fe_{0.7}Co_{0.3}O_{3-\delta}$ perovskite as cathode material for ITSOFCs," *Solid State Ionics*, 2002, 147, pp.41-48.
6. M.Feng, and J. B. Goodenough: "A superior oxide-ion electrolyte," *Eur. J. Solid State Inorg. Chem*., 1994, 31, pp.663-672.

7. H. Hu and M. Liu: "Interfacial Studies of Solid State Cells Based Electrolytes of Mixed Ionic-Electronic Conductors," *Solid State Ionics*, 1998, Vol. 109/3-4, pp. 259-277.
8. S. Wang, X. Lu and M. Liu: "Electrocatalytic properties of LSM-based electrodes for oxygen reduction," *J. of Solid State Electrochemistry,* 2002, Vol 6, pp. 384-390.
9. S.B. Adler: "Mechanism and kinetics of oxygen reduction on porous $La_{1-x}Sr_xCoO_{3-\delta}$ electrodes," *Solid State Ionics,* 1998, 111, pp. 125–134.
10. Paola Costamagna, Paolo Costa and Vincenzo Antonucci: "Micro-modelling of solid oxide fuel cell electrodes," *Electrochimica Acta,* 1998, 43, pp. 375-394.
11. A. Barbucci, R. Bozzo, G. Cerisola and P. Costamagna: "Characterisation of composite SOFC cathodes using electrochemical impedance spectroscopy. Analysis of Pt/YSZ and LSM/YSZ electrodes," *Electrochimica Acta,* 2002, 47, pp. 2183-2188.
12. J. E. Bauerle: "Study of Solid Electrolyte Polarization by a Complex Admittance Method," *J. Phys. Chem. Solids*, 1969, 30, pp. 2657-70.
13. R. Macdonald: Impedance Spectroscopy: Emphasizing Solid Materials and Systems, Wiley, New York, 1987.
14. T. Kenjo, S. Osawa, and K. Fujikawa: "High Temperature Air Cathodes Containing Ion Conductive Oxides," *J.Electrochem. Soc.,* 1991, 138, pp.349-355.
15. C.W. Tanner, K.Z. Fung and A.V. Virkar: "The Effect of Porous Composite Electrode Structure on Solid Oxide Fuel Cell Performance. I. Theoretical Analysis," *J. Electrochem. Soc.,* 1997, 144, pp.21-30.
16. A.V. Virkar, J.Chen, C.W. Tanner and J.W. Kim: "The role of electrode microstructure on activation and concentration polarizations in solid oxide fuel cells," *Solid State Ionics,* 2000, 131, pp. 189–198.
17. Teruhisa Horita, Katsuhiko Yamaji, Natsuko Sakai, Yueping Xiong, Tohru Kato, Harumi Yokokawa and Tatsuya Kawada: "Determination of proton and oxygen movements in solid oxides by the tracer gases exchange technique and secondary ion mass spectrometry," *Applied Surface Science,* 2003, 203-204, pp. 634-638.
18. Meilin Liu and Zhonglin Wu: "Significance of interfaces in solid-state cells with porous electrodes of mixed ionic–electronic conductors," *Solid State Ionics,* 1998, 107, pp. 105-110.
19. *S. B. Adler, J. A. Lane, B. C. H. Steele: "*Electrode Kinetics of Porous Mixed-Conducting Oxygen Electrodes," *J. Electrochem. Soc.,* 1996, 143, pp. 3554–3564.
20. J.P.P. Huijsmans, F.P.F. Berkel and G.M. Christie: "Intermediate temperature SOFC – a promise for the 21st century," *J. Power Sources,* 1998, 71, pp. 107-110.
21. M. Feng, J.B. Goodenough, K. Huang and C. Milliken: "Fuel cells with doped lanthanum gallate electrolyte," *J. Power Sources,* 1996, 63,pp. 47-51.

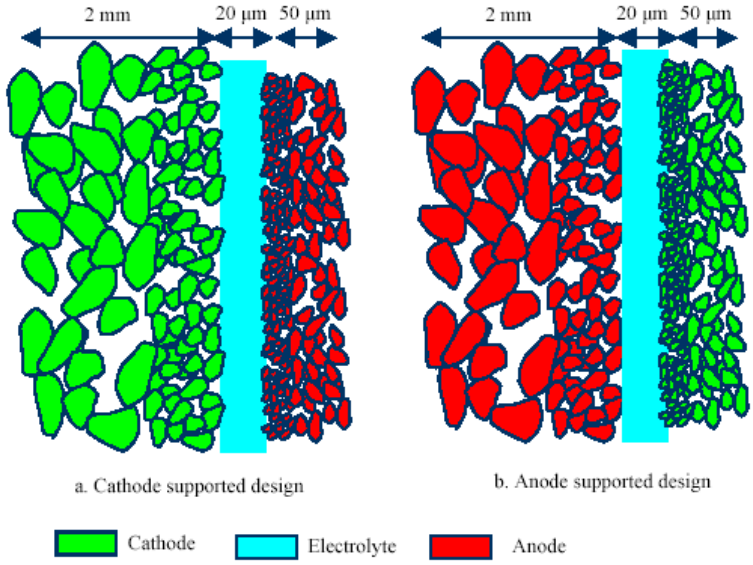

Fig. 1. Schematic of electrode-supported SOFCs

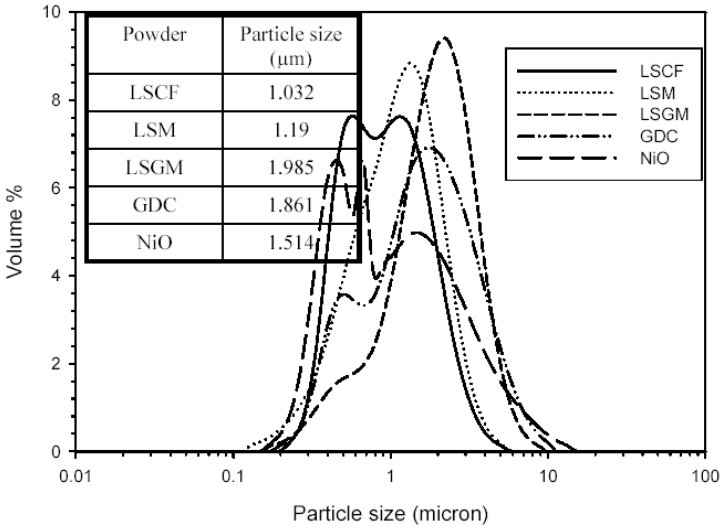

Fig. 2. Final particle size distribution of the synthesized powders

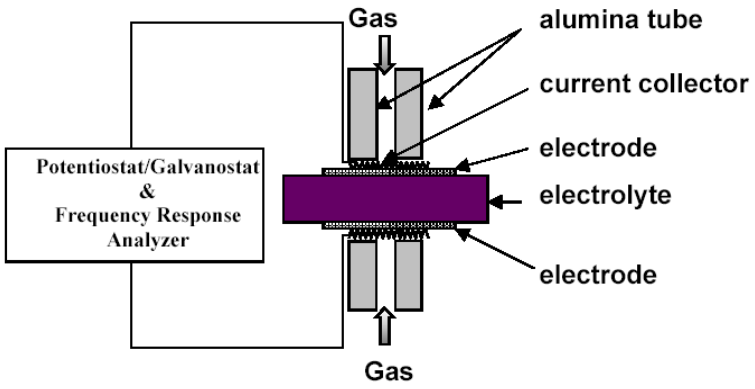

Fig. 3. Schematic of the experimental setup for impedance measurement

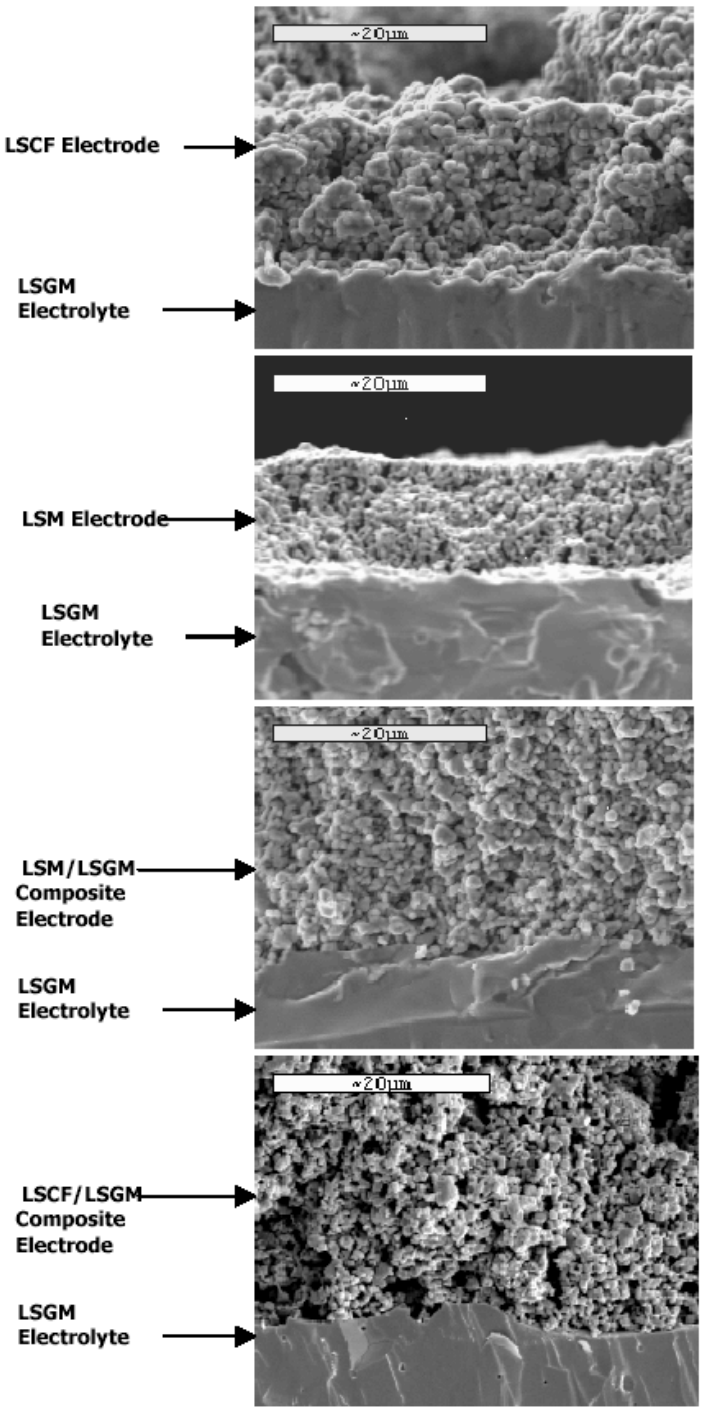

Fig. 4. SEM micrographs of fracture surfaces of (a, top) LSCF/LSGM interface, (b, middle) LSM/LSGM interface, (c, middle) LSM-LSGM/LSGM interface, (d, bottom) LSCF-LSGM/LSGM interface.

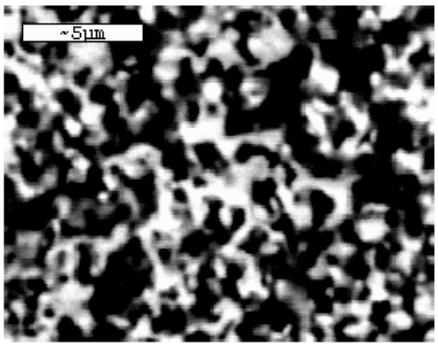

(a)

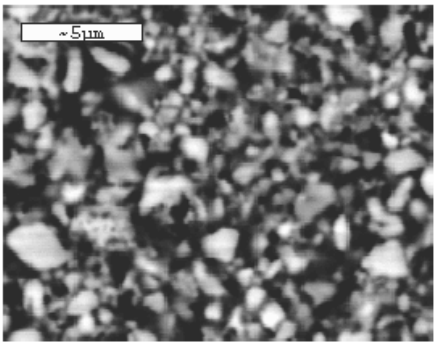

(b)

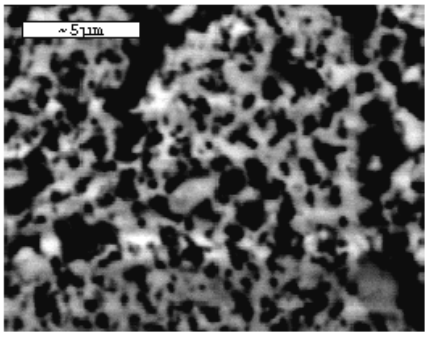

(c)

Fig. 5. Back scattered SEM micrographs of polished surfaces of (a, top) LSM electrode, (b, middle) LSM-LSGM electrode, (c, bottom) LSCF electrode.

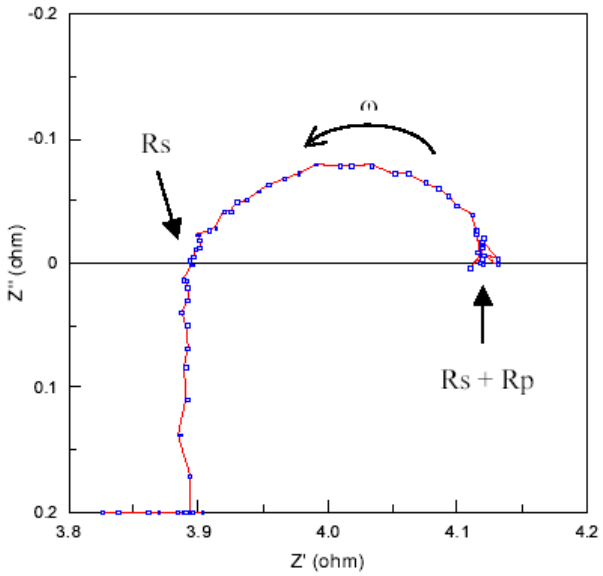

Fig. 6. A typical impedance of symmetrical LSCF/LSGM/LSCF cell in air at 800°C.

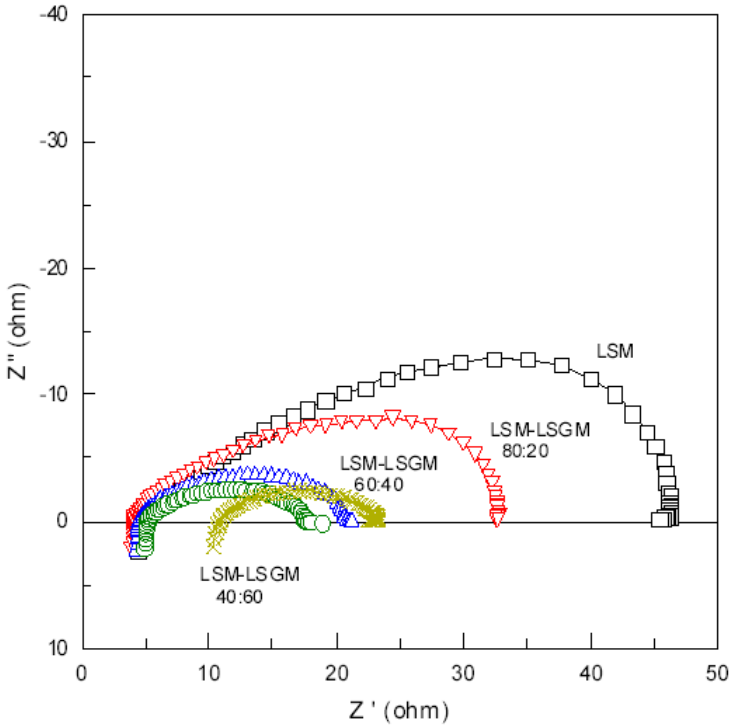

Fig. 7. Typical impedance spectra of symmetrical LSM-LSGM/LSGM'LSM-LSGM cells with different LSM-LSGM compositions measured in air at 800°C.

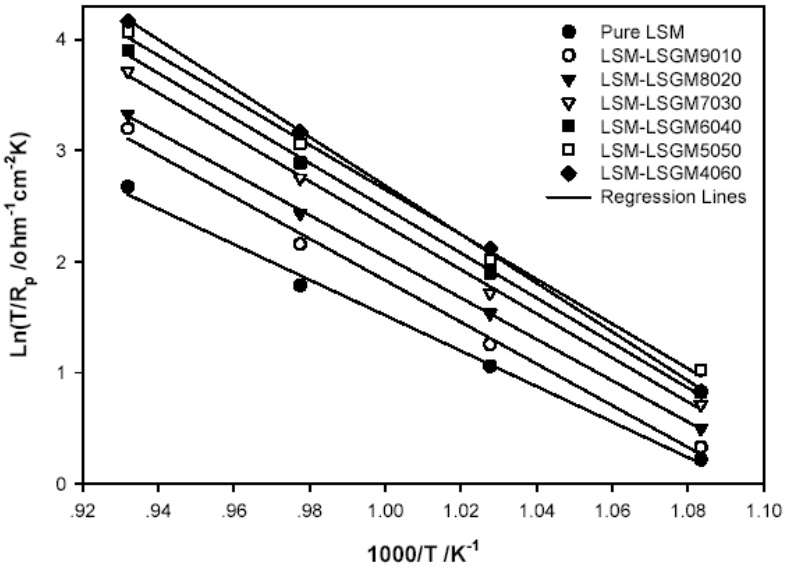

Fig. 8. Temperature dependence of the polarization resistance for different LSM-LSGM compositions measured in air.

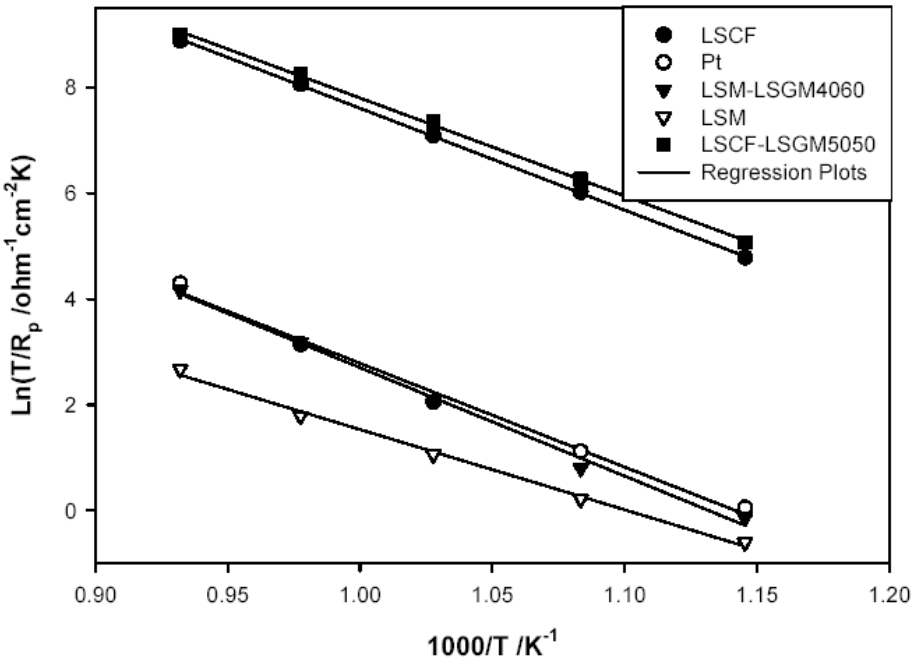

Fig. 9. Temperature dependence of the polarization resistance for various cathode materials measured in air.

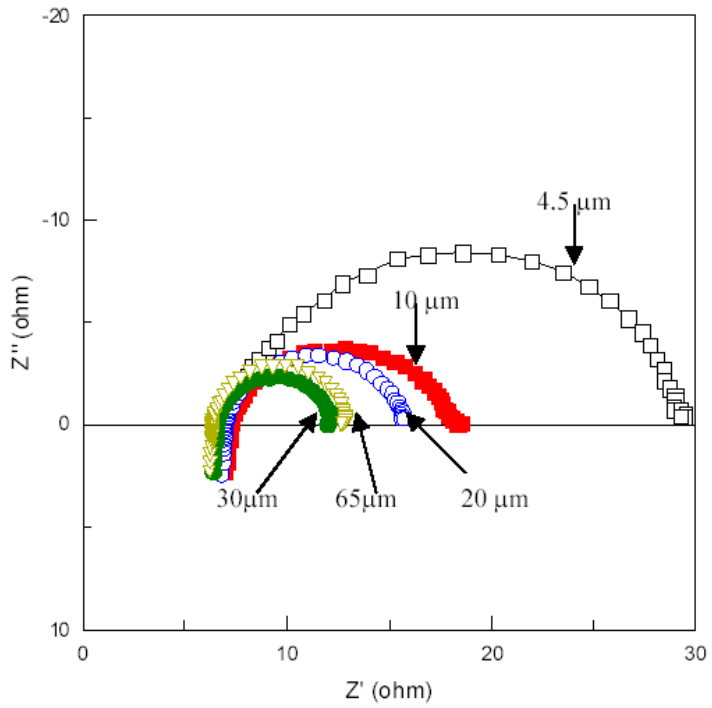

Fig. 10. Impedance spectra of symmetrical LSCF/LSGM/LSCF cells with various electrode thickness measured in air at 600°C.

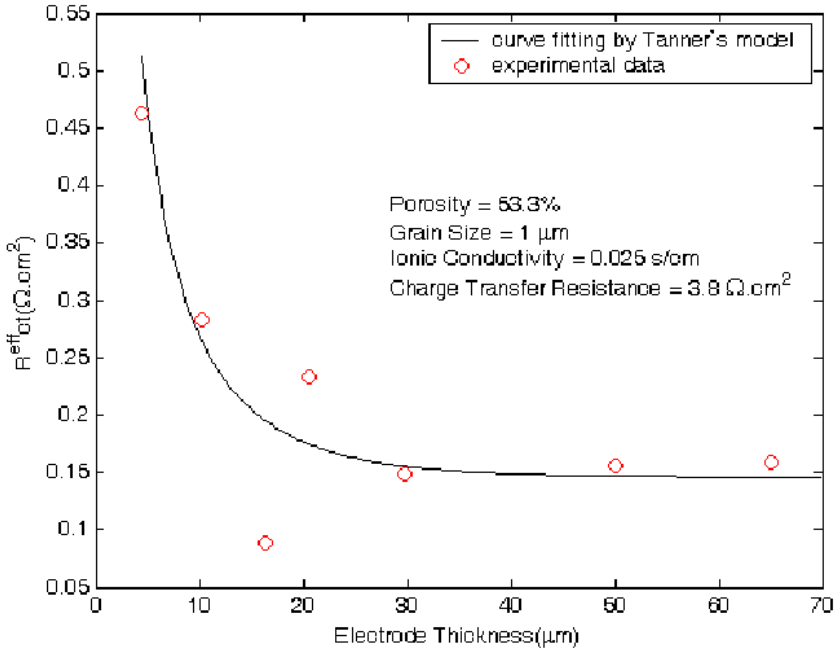

Fig. 11. A plot of charge transfer resistance as a function of electrode thickness for symmetrical LSCF/LSGM/LSCF cells measured in air at 800°C.

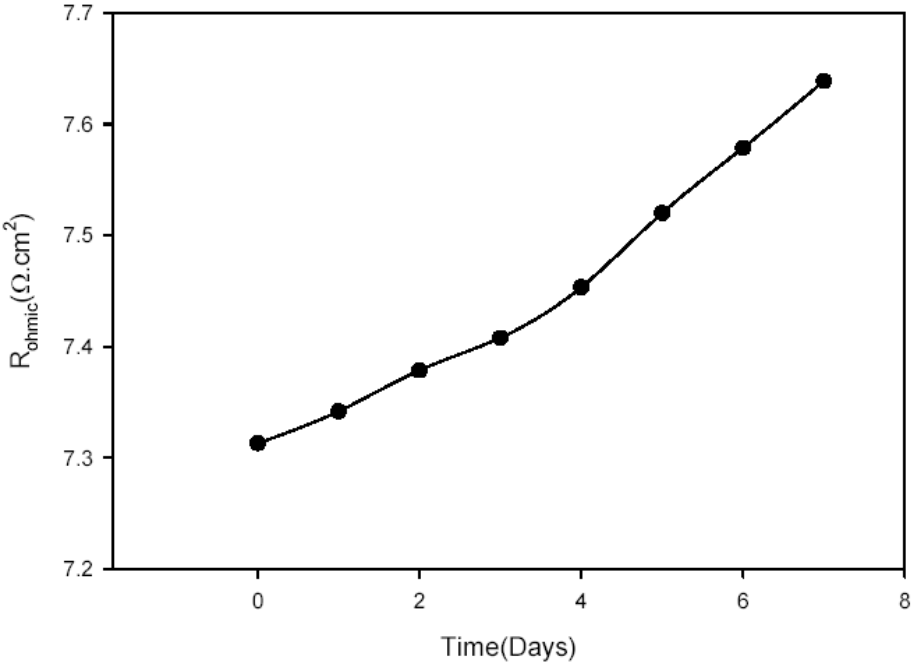

Fig. 12. Time dependence of ohmic resistance of symmetrical Ni-GDC/LSGM/Ni-GDC cell measured in reducing atmosphere at 800°C.

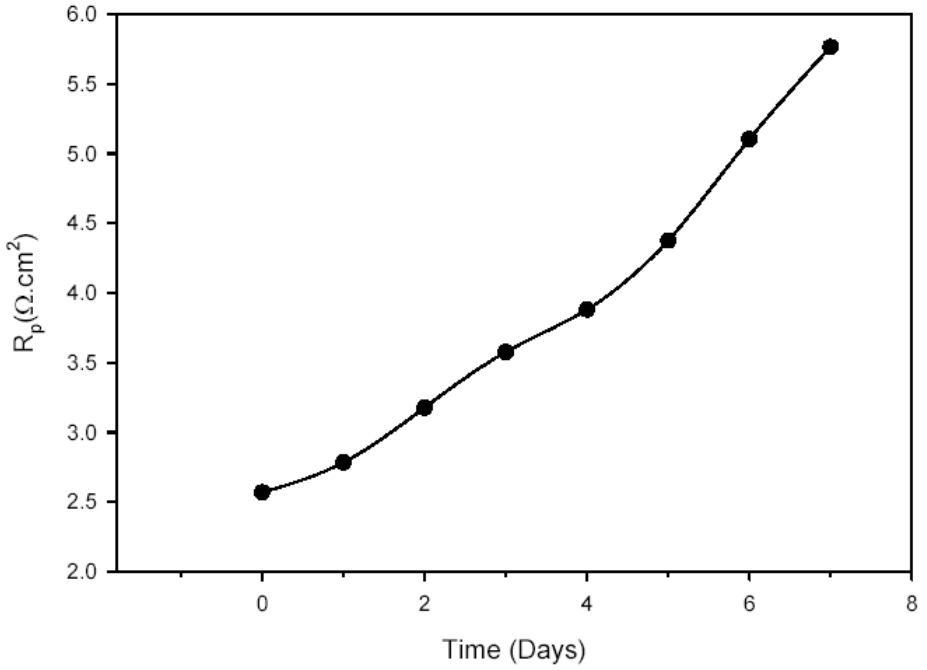

Fig. 13. Time dependence of polarization resistance of symmetrical Ni-GDC/LSGM/Ni-GDC cell measured in reducing atmosphere at 800°C.

Electrode materials	Pt	LSM	LSM-LSGM	LSCF	LSCF-LSGM	Ni-GDC
Composition	Pure Platinum	Pure $La_{0.9}Sr_{0.1}MnO_3$	$La_{0.9}Sr_{0.1}MnO_3$ +$La_{0.9}Sr_{0.1}Ga_{0.8}Mg_{0.2}O_3$	Pure $La_{0.6}Sr_{0.4}Co_{0.8}Fe_{0.2}O_3$	$La_{0.6}Sr_{0.4}Co_{0.8}Fe_{0.2}O_3$ +$La_{0.9}Sr_{0.1}Ga_{0.8}Mg_{0.2}O_3$	Ni +$Ce_{0.85}Gd_{0.15}O_2$
Thickness (μm)	5	30	30	4.5 ~ 150	30	30

Table. 1. The list of electrode materials investigated and the respective thickness.

	Pure LSM	**LSM-LSGM 90:10**	**LSM-LSGM 80:20**	**LSM-LSGM 70:30**	**LSM-LSGM 60:40**	**LSM-LSGM 50:50**	**LSM-LSGM 40:60**
Ea (KJ/mol)	126	156	155	165	168	167	182

Table. 2. Activation energies of LSM-LSGM composite electrodes on LSGM electrolyte.

	Pure LSM	**LSM-LSGM 40:60**	**Platinum**	**LSCF**	**LSCF-LSGM 50:50**
Ea (KJ/mol)	**126**	**182**	**163**	**165**	**154**

Table. 3. Activation energies of investigated cathodes on LSGM electrolyte.